



AMPLITUDE AND FREQUENCY MODULATION OF THE SMALL SCALES IN A TURBULENT JET

D. Fiscaletti

Lab. for Aero & Hydrodynamics
Department of Mechanical Engineering
Delft University of Technology
Leeghwaterstraat 21 2628 CA Delft, The Netherlands
d.fiscaletti@tudelft.nl

G.E. Elsinga

Lab. for Aero & Hydrodynamics
Department of Mechanical Engineering
Delft University of Technology
Leeghwaterstraat 21 2628 CA Delft, The Netherlands
g.e.elsinga@tudelft.nl

B. Ganapathisubramani

Aerodynamics and Flight Mechanics Research Group
University of Southampton
SO17 1BJ
g.bharath@soton.ac.uk

J. Westerweel

Lab. for Aero & Hydrodynamics
Department of Mechanical Engineering
Delft University of Technology
Leeghwaterstraat 21 2628 CA Delft, The Netherlands
j.westerweel@tudelft.nl

This work involves the large-scale amplitude and frequency modulation of the small-scale motions in fully-developed turbulence of a high Reynolds number jet. The scales responsible for the production of turbulent kinetic energy (large scales), and those responsible for its viscous dissipation (small scales) are extracted from time series of hot-wire signals, using a band-pass spectral filter. The top-down interaction between the turbulent scales is then examined. We show that the strength of the large-scale fluctuations affect non-linearly the amplitude of the small-scale signal. Furthermore, the higher frequency components within the small-scale signal exhibit stronger amplitude modulation, which evidences frequency modulation. Analogies and dissimilarities with turbulent flows other than jets are discussed.

INTRODUCTION

Many recent studies have shown the existence of a clear relationship between the large-scale motions and the small-scale motions in turbulent boundary layers (1) (2)

(3). The extent of this scale interaction was later quantified, based on correlation coefficients (4). However, the correlation coefficient exhibits a linear trend with the skewness of the raw signals, and therefore does not represent a tool independent of the data that is analyzed (5). To overcome this limitation, the use of two-point amplitude modulation correlation was suggested (6). Although an interaction between the scales could be quantified eventually, the correlations proposed did not take into account the different contributions of the large-scale fluctuations on the amplitude modulation. Recently, this gap was filled following the development of an original approach based on signal binning (7). Furthermore, independently of an amplitude modulation, a frequency modulation of the small-scale motions was ascertained too (7).

Despite the interaction between the large-scale and small-scale motions has recently aroused a deep interest, shear flows other than boundary layers have been scarcely tackled in literature. Only a mixing layer at a low Reynolds number has been investigated so far (8). In addition, frequency modulation of the small-scale motions is of novel

finding, thus worthy to be investigated more in details.

Therefore, the main goal of the present work is to extend the work on amplitude and frequency modulation to jets, and compare the results to those for boundary layers and mixing layers reported in the literature. In particular, at the jet centerline, the mean shear vanishes, which is an important difference with respect to other flows considered so far. A secondary goal of this study is to develop a mathematical approach that can provide a further insight into the physics behind the scale interaction, with a particular focus on frequency modulation (7).

EXPERIMENTAL DATASET

Velocity signals were measured in a circular jet in air using a CTA. Data were recorded at a downstream distance of $x/D = 70$ from the nozzle, in the self-similar region over a range of radial positions. The governing non-dimensional numbers at the nozzle, whose diameter is $D = 8$ mm, can be estimated as $Re = 6.6 \cdot 10^4$ and $Ma = 0.37$. The jet centerline velocity U_c at $x/D = 70$ is 10.55 m/s, and the jet's half width at that location is 52 mm. The measurements were performed with an overheat adjustment of 0.7, in order to keep the temperature of the sensor at a constant temperature of 220°C. The sensor was a Dantec 55P11. The radial locations of measure ranged from 0 to 0.2 non-dimensional radii, where the normalization was done with respect to the jet's half width. The range of interest was deliberately restricted to the proximity of the centerline position in order not to enter the intermittent region of the jet. The feedback control of the wire temperature was established through a Dantec Dynamics 56C17 CTA Bridge.

From the following relationship, an estimate of the dissipation rate in jets is provided (9):

$$\varepsilon \approx 0.015 \frac{U_c^3}{r_{1/2}} \quad (1)$$

where U_c is the centerline velocity and $r_{1/2}$ is the jet's half-width. Based on the dissipation rate at the mentioned measurement location, the size of the Kolmogorov scales is estimated to be around 60 μm , which corresponds to a frequency of 30 kHz at the jet centerline when employing Taylor's hypothesis. Since for frequencies higher than 22 kHz the measurement noise dramatically affects the signal, a low-pass filtering at this cutoff frequency has to be applied. As a consequence, the minimum size of the eddies that the measurement can resolve is estimated at 90 μm , corresponding to about 1.5 Kolmogorov length scales.

MATERIAL AND METHODS

In Figure 1, the velocity power spectrum is shown. The -5/3 trend in the inertial range of the energy cascade develops over two decades: this demonstrates the highly turbulent nature of the flow, and an adequate separation of the large scales, and small scales. Moreover, the large scales, which are dominated by turbulent kinetic energy, can be clearly distinguished from the small scales that are dominated by dissipation. In Figure 1, we present the two frequency bands of the power spectrum, which are taken to be representative of the large-scale signal (red) and the small-scale signal (green). In particular, the low-frequency signal contains scales that range between 2λ and L , where λ is the

size of the Taylor length scale (2.15 mm), and L the size of the eddies comparable to the flow scale (43 mm). Here, an estimate of the Taylor length was obtained from the given relationship (10):

$$\lambda = u' \sqrt{15 \frac{\nu}{\varepsilon}} \quad (2)$$

where u' is the RMS of the axial velocity. In the fully-developed region of a jet flow, and for the radial range explored in the present work, we can assume $u' \approx 0.25 \cdot U_c$ (11). Moreover, L was estimated as follows:

$$L \sim \eta \cdot Re^{3/4} \quad (3)$$

Thus, the high-frequency signal contains scales from 1.5η and 5η , where η is the Kolmogorov scale. The physical meaning of the ranges chosen for the scale separation is confirmed by analysing the dissipation spectrum, shown in Figure 2. The two pass-band ranges are on the two different tails of the bell.

The frequency bands representative of the large and the small scales were thus determined. Later, a spectral band-pass filter allowed to separate the large-scale and the small-scale contributions from the original broadband velocity signal.

RESULTS AND DISCUSSION

A portion of the velocity signal is presented in Figure 3, together with the corresponding large-scale and small-scale components, obtained as described in the previous section. The signal was acquired at the centerline position, therefore far from the mean shear region. Even without computing any statistics, the small-scale signal fluctuations (green) are clearly broader when the large-scale fluctuations (red) are positive. On the other hand, the small-scale signal becomes much flatter for negative fluctuations of the large-scale component. Evidently, the viscous scales are affected by the large-scale motions, and, indeed, the scales responsible for the production of the turbulent kinetic energy have a role in modulating the amplitude of the dissipative scales. This trend is more evident in Figure 4, where the probability density functions (pdfs) of the small-scale signals conditioned on the sign of the large-scale fluctuations are presented. In particular, only the large-scale fluctuations higher in absolute value than the large-scale signal rms have been taken into consideration in the estimate of the pdfs of the small-scale signal fluctuations. The variance of the pdf conditioned on the positive fluctuations of the large-scale signal is higher than the one for the negative large scale fluctuations: this clearly demonstrates that the presence of large eddies has a modulating effect on the small-scale turbulent activity.

Nevertheless, the variance of the conditioned pdf does not provide a detailed dependence between the strength of the large-scale signal, and the amplitude modulation of the small-scale motions. Hence, a mathematical procedure similar to that detailed in (7) was developed, and applied to the present experimental dataset. In the following, we refer to u_L^* as the fluctuations of the large-scale signal non-dimensionalized by the average centerline velocity U_c . Therefore, $u_L^* = u_L/U_c$. The aforementioned procedure consists of the following steps:

- i. Equally spaced bins with a spacing of 0.05 ranging from $u_L^* = -0.4$ to $u_L^* = 0.4$ were created. A bin spacing of 0.05 was chosen as a balance between the bin size, and the number of samples within each bin. With such a size of bin, the minimum amount of samples falling within each bin was higher than 1000.
- ii. Each large-scale sample corresponds to a small-scale sample at the same instant in time.
- iii. Each sample of the small-scale signal was included in a group, corresponding to one of the u_L^* bins, effectively creating a single new time series for each u_L^* bin.
- iv. The variance of the samples contained in each group was then computed, and this small-scale variance represents the amplitude of the small scales conditioned on the strength of the respective large-scale signal, σ_{u_L} . The variance was non-dimensionalized by the variance of the entire small-scale fluctuations at the centerline σ_c , therefore, $\sigma_{u_L}^* = \sigma_{u_L} / \sigma_c$.

Furthermore, the approach by Ganapathisubramani *et al.* was applied too (7), in order to allow a comparison. A binning with a spacing of 0.05 ranging from $u_L^* = -0.4$ to $u_L^* = 0.4$ was again created for the large-scale fluctuations. Moreover, in compliance with the algorithm, the time series of both the large- and the small-scale fluctuations were divided into segments of 100 samples each (corresponding to $5 \cdot 10^{-4}$ s). This segment size was chosen as the ratio between the acquisition frequency and 2001Hz, a frequency intermediate between the large and the small-scale motions. With such a size of bin and horizontal segment, the minimum amount of samples falling within each bin was 400. Figure 5 shows the results obtained after applying the present procedure, and the literature procedure, respectively, to the signal acquired at the centerline. Evidently, although different, the two algorithms produced similar results. The small deviation between the two plot lines is probably due to a lack of statistical convergence in the procedure from literature. The variance over one segment (blue line) does not converge to the variance computed over all the small-scale samples (red line). The lack of statistical convergence creates an offset between the two plot lines. Even if not shown here, this offset is witnessed to increase for decreasing sizes of the horizontal segments, as expected. The amplitude modulation effects are linear for fluctuations of the large-scale signal close to zero. Nevertheless, the interaction between the large- and the small-scale motions is generally non-linear. Similarly, analogous graphs are obtained over the range of different radial positions from 0 to 0.2 non-dimensional radii. In Figure 6, the two procedures are applied to a signal taken at the radial location of 0.2 non-dimensional radii. Even if at negative fluctuations of the large-scale signal the plot line is flatter, the trend is clearly the same as at the centerline. This is consistent with (3), where the correlation coefficient between the large-scale signal, and the envelope of the small-scale signal are observed to remain constant across different radial positions.

Moreover, the frequency modulation of the small-scale motions is checked. In particular, we want to show that the amount of amplitude modulation depends on the frequency of the small-scale signal. In this study, an approach different to that proposed in literature ((7)) is used. Firstly, the frequency band representative of the dissipative scales in the power spectrum is further subdivided into four smaller frequency bands of equal sizes, as shown in the inset of Figure 7. Secondly, the procedure described by Ganapathisub-

ramani *et al.* (7) for the estimate of the amplitude modulation is applied to the four different small-scale signals (Figure 7). Additionally, the resulting values of the variance are non-dimensionalized by the respective variances at zero u_L^* to compensate for differences in the energy contained in the frequency bands. For every signal, the variance at zero is calculated as an average between the two variances of the small-scale fluctuation for $0 < u_L^* < 0.05$ and $-0.05 < u_L^* < 0$. In Figure 8, the results are presented. As the large-scale signal exhibits positive fluctuations, the highest normalized variance is always obtained for the signal of the highest frequency band (black). In general, when the Kolmogorov scales are approached, the rate of amplitude modulation with the strength of the large-scale signal increases. As a matter of fact, the slope of the positive branches of the plot lines rises for signals corresponding to increasing frequencies. In other words, the activity of the large-scale motions stimulates the viscous scales of the turbulence more in frequency intervals next to the upper limit of the dissipative band, than at the lower frequencies. A similar trend was observed at different radial positions, for non-dimensional radii ranging between 0 and 0.2, even if not shown here. These results have some physical implications. The activity of the large-scale motions modulates the amplitude of the small-scale signal in various ways, depending on the frequency of the small-scale signal (frequency modulation). As a consequence, the behaviour of the large scales alter the shape of the velocity power spectrum locally. In particular, the small-scale frequency band becomes flatter for positive fluctuations of the large-scale signal, and steeper for negative fluctuations. In order to show this, the following procedure was implemented.

- i. Firstly, the small-scale signal was divided into smaller segments of 200 samples each, corresponding to 10^{-3} s.
- ii. A hamming filter was applied to the segments of the small-scale signal.
- iii. From all the filtered segments, we selected only those with a wanted u_L^* in the corresponding large-scale signal.
- iv. Ten-by-ten, the selected pieces of the small-scale signal were juxtaposed, thus generating new signals.
- v. The power spectra for each of these ten-segments signals were calculated. Additionally, the average power spectrum was computed. Finally, the obtained average power spectrum was normalized by its value at $k\eta = 10^{-0.6}$, to compensate for the differences in the energy content.

The detailed scheme was applied for three different u_L^* . The results are shown in Figure 10. The power spectrum was firstly conditioned on representatives of the large-scale fluctuations ranging between 0.3 and 0.35 (red line), then between -0.3 and -0.35 (green line), and, eventually, for randomly selected segments of the small-scale signal (unconditional u_L^* , blue line). As expected, the slope of the green line (negative fluctuations) is the highest, whereas the slope of the red line (positive fluctuation) is the lowest. Again, this proves that the amplitude modulation of the small-scale signal is frequency dependent, and that the degree of amplitude modulation increases at higher frequencies. The described scenario can be explained in terms of energy cascade mechanism. Positive fluctuations of the large-scale signal produce additional turbulent kinetic energy, that is later dissipated by the increased activity of the viscous scales.

The correlation coefficient (R) between the large-scale and the envelope of small-scale signal reinforces the above hypothesis. The envelope of the small-scale signal is calculated following the approach by Mathis *et al.* (4). The Hilbert transform was firstly applied to the small-scale signal. For the envelope, we filtered the Hilbert-transformed signal using the same spectral filter as for the large-scale fluctuations. Additionally, we calculate the correlation coefficient R for different mutual delays of the two signals. As a convention, a positive time shift is equivalent to delaying the large-scale signal. In Figure 9, the result of this procedure is shown. The maximum correlation coefficient ($R = 0.65$) is found for a negative shift of $1.8 \cdot 10^{-4}$ s, almost equal to the Kolmogorov time scale $\tau_\eta = 2 \cdot 10^{-4}$ s. Therefore, a negative shift implies a delay in the top-down interaction. This delay can be regarded as the time necessary by the turbulent kinetic energy to transfer from the large-scale to the dissipative-scale motions.

These findings could be put in relationship with the evidence of scale interactions found in other shear flows, such as boundary layers, and mixing layers. In boundary layers, a behaviour analogous to the one presented here is reported in proximity to the wall ($u_L^* > 0$, $\sigma_{u_L}^* \uparrow$) (7). On the other hand, moving away from the wall (i.e., in the wake region), the opposite phenomenon is reported ($u_L^* > 0$, $\sigma_{u_L}^* \downarrow$). With regard to mixing layers, Buxton shows that a damping effect is exerted on the small-scale fluctuations by the large-scale positive fluctuations (12). In other words, high-frequency velocity fluctuations strengthen on average for negative values of the large-scale signal ($u_L^* > 0$, $\sigma_{u_L}^* \downarrow$), similar to the wake region of the turbulent boundary layer. Evidently, both the type of the flow investigated, and the position where the acquisition is performed play a decisive role in the small-scale amplitude modulation. The different ways in which the large scales organize themselves may explain the aforementioned different behaviours (3).

Recently, the dissipation of more than a half of the turbulent kinetic energy was observed to occur in regions of intense shear, between pairs of tube vortices (13) (14). According to these investigations, the activity of the small scales is exalted in the layer between travelling large eddies, which has been argued to be a universal feature of turbulent motions (15). We expect that regions of sharp gradients in the large-scale velocity fluctuations might be characterized by a high energy content at the viscous scales. Therefore, rather than the large-scale fluctuations, the large-scale velocity gradients can play a determinant role in modulating the viscous scales. In this case, the relationship between the large-scale velocity gradients and the small-scale signal could be univocal, independently of the turbulent flow under investigation.

CONCLUSIONS

In this study, we examined the top-down interaction between the large, and the small-scale motions in the far field turbulence of an air jet, at high Reynolds number. Time series of hot-wire signals were regarded as space resolved data, after applying the Taylor's hypothesis. The velocity signals were decomposed into large-scale and small-scale contributions, using a spectral filter. The impact of the large-scale components on the viscous scales was investigated. The experimental dataset was evaluated through several different metrics, both existing and newly developed. It was found that the small-scale motions are modulated

both in amplitude and frequency. The described modulating behaviour was ascertained for different radial positions within the jet. Using an approach analogous to that shown by Ganapathisubramani *et al.* (7), we quantified the nonlinear contributions of the large-scale fluctuations to the amplitude modulation. Moreover, a spectral decomposition of the small-scale signal evidenced that the amplitude modulation is frequency dependent. In particular, the viscous scales are more amplitude modulated when approaching the Kolmogorov scale.

Although the literature on scale interaction is limited, the present results on jets could be related to the findings over different turbulent flows. A behaviour similar to that here shown was evidenced in boundary layers, in proximity to the wall. But, moving towards the outer region of the boundary layer, a phase reversal was reported. A similar phase reversal was observed in mixing layers. This difference in the scale coupling may be explained in terms of large-scale organization. Evidently, the modulation of the small-scale signal is strongly flow dependent, and it even varies between different positions within the same flow (e.g., in turbulent boundary layers). This suggests that the scale interaction is intimately related to the way the large-scale structures arrange themselves within the flow.

Nevertheless, the top-down interaction between scales was expected to be independent of the flow under investigation. Therefore, it is probably deceptive to directly relate the small-scale to the large-scale signal. In agreement to the recent literature, shear regions with high velocity gradients are responsible for the largest amount of energy dissipation, hence small-scale activity. In future works, the interaction between large-scale velocity gradient and the small-scale signal should be explored. In the top-down interaction between scales, we expect to find a common behaviour in all the turbulent flows.

References

- [1] Hutchins N. and Marusic I. Evidence of very long meandering features in the logarithmic region of turbulent boundary layers. (2007) *J. Fluid Mech.* **579**, 1–28.
- [2] Hutchins N. and Marusic I. Large-scale influences in near-wall turbulence. *Phil. Trans. R. Soc. A* **365**, 647–664.
- [3] Bandyopadhyay P.R. and Hussain K.M.F. The coupling between scales in shear flows. (1984) *Phys. Fluids* **27**.
- [4] Mathis R., Hutchins N. and Marusic I. Large-scale amplitude modulation of the small-scale structures in turbulent boundary layers. (2009) *J. Fluid Mech.* **628**, 311–337.
- [5] Schlatter P. and Örlü R. Quantifying the interaction between large and small scales in wall-bounded turbulent flows: A note of caution. (2010) *Phys. Fluids* **22**.
- [6] Bernardini M. and Pirozzoli S. Inner/outer layer interactions in turbulent boundary layers: A refined measure for the large-scale amplitude modulation mechanism. (2011) *Phys. Fluids* **23**.
- [7] Ganapathisubramani B., Hutchins N., Monty J.P., Chung D. and Marusic I. Amplitude and frequency modulation in wall turbulence. (2012) *J. Fluid Mech.*, **708**, 1–31.
- [8] Buxton O.R.H. Fine scale features of turbulent shear flows. (2011) PhD thesis, Imperial College London.

August 28 - 30, 2013 Poitiers, France

- [9] Panchapakesan N.R. and Lumley J.L. Turbulence measurements in axisymmetric jet of air and helium. part 1. air jet. (1993) *J. Fluid Mech.* **246**, 197–223.
- [10] Taylor G.I. Statistical theory of turbulence: Parts I-III. (1935) *Proc. R. Soc. London Ser. A* **151**, 421–464.
- [11] Hussein H.J., Capp S., and George W.K. Velocity measurements in a high-Reynolds-number, momentum-conserving, axisymmetric, turbulent jet. (1994) *J. Fluid Mech.* **258**, 31–75.
- [12] Buxton O.R.H. and Ganapathisubramani B. Scale interactions in the far-field of a turbulent mixing layer. *private communication*
- [13] Ganapathisubramani B., Lakshminarasimhan K., and Clemens N.T. Investigation of three-dimensional structure of fine scales in a turbulent jet by using cinematographic stereoscopic particle image velocimetry. (2008) *J. Fluid Mech.* **598**, 141–175.
- [14] Goto S. A physical mechanism of the energy cascade in homogeneous isotropic turbulence. (2008) *J. Fluid Mech.* **605**, 355–366.
- [15] Elsinga G.E., and Marusic I. Universal aspects of small-scale motions in turbulence. (2010) *J. Fluid Mech.* **662**, 514–539.

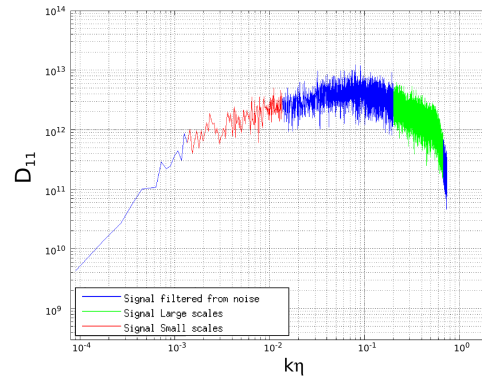


Figure 2. Dissipation spectrum of the signal at the jet centerline, $D_{11} = k^2 \cdot P_{11}$

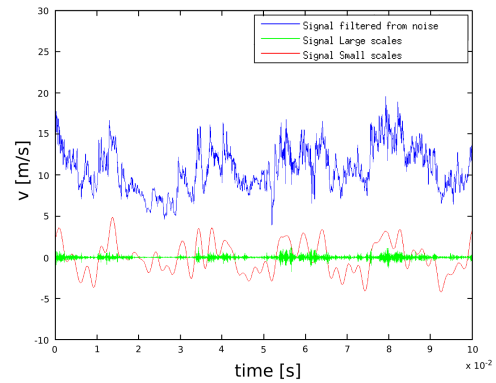


Figure 3. Velocity signal (blue), small-scale (green), and large-scale (red) components of the velocity signal.

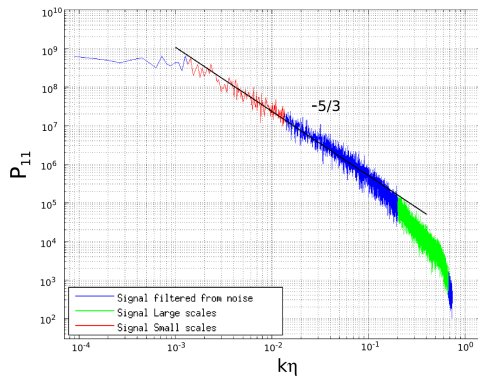


Figure 1. Power spectrum of the signal taken at the jet centerline ($x/D = 70$)

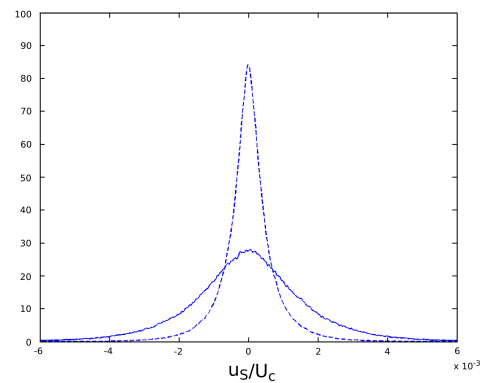


Figure 4. Pdf of the small-scale fluctuations, conditioned on the positive (solid line), and negative (dashed line) fluctuations of the large-scale signal.

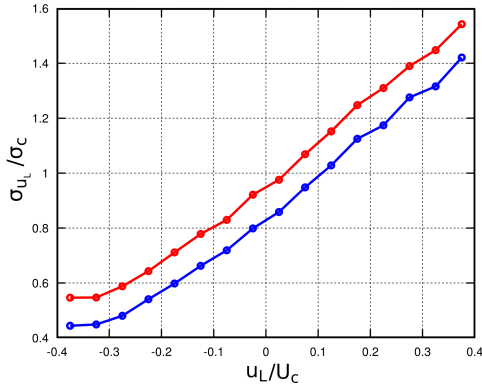


Figure 5. Variance of the pdf of the small-scale signal, conditioned on the fluctuations of the large-scale signal. The signal is acquired at the centerline position, at $x/D = 70$. The two procedures applied are described in the Result section (red line), and in (7) (blue line).

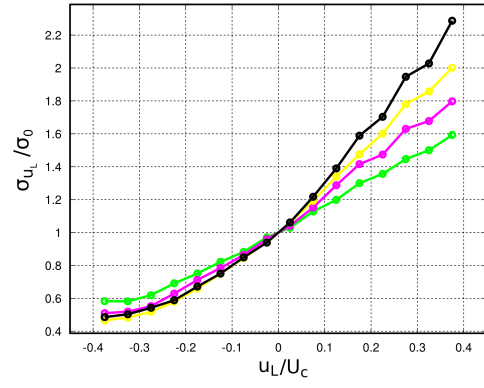


Figure 8. Normalized variances of the pdf of the four small-scale signals, conditioned on the fluctuations of the large-scale signal. The colours correspond to the frequency band (Figure 7) considered for the filtering.

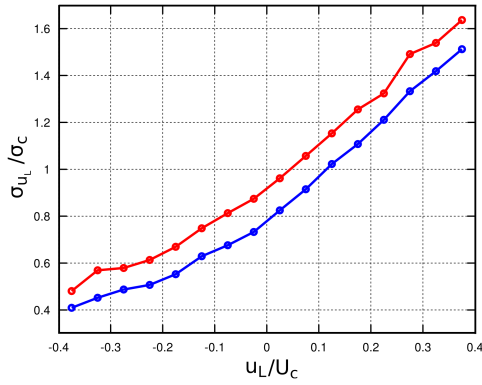


Figure 6. Variance of the pdf of the small-scale signal, conditioned on the fluctuations of the large-scale signal. The radial location of the measure is 0.2 non-dimensional radii. The two procedures applied are described in the Result section (red line), and in (7) (blue line).

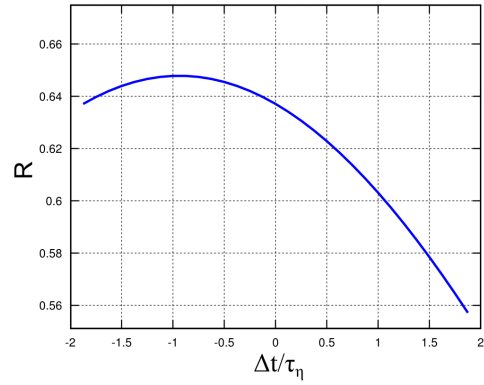


Figure 9. Correlation coefficients R for different values of the relative shift between the signals correlated, after applying the approach by Mathis *et al.*(4).

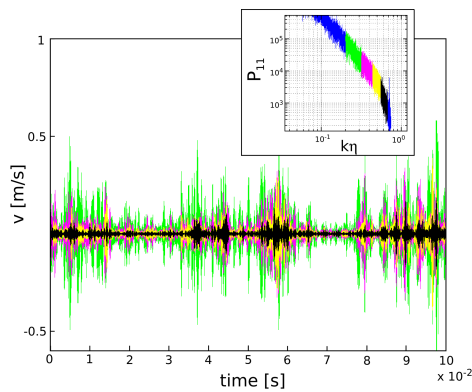


Figure 7. In the inset, the small-scale range of the power spectrum is divided into four different frequency bands, evidenced through different colours. In the picture, small-scale signals obtained from the four different frequency bands, as evidenced in the inset.

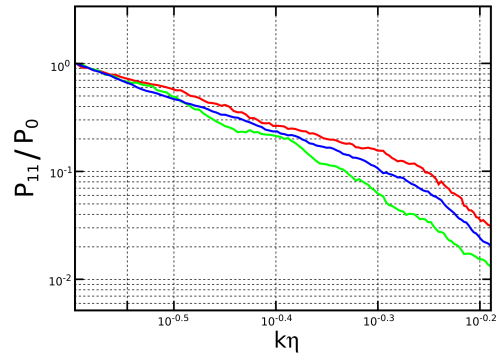


Figure 10. Power spectra of conditionally selected segments of the small-scale signal. The red line is obtained for u_L^* ranging between 0.3 and 0.35, the green line between -0.3 and -0.35 , and the blue line is obtained for unconditional u_L^* (randomly selected segments of the small-scale signal). The scheme adopted in computing the different power spectra is detailed in the Result section.